INL/CON-19-56932-Revision-1

Electromagnetic Shielding Design for 200 kW Stationary Wireless Charging of Light-Duty EV

Bo Zhang, Richard Barney Carlson, Veda P. Galigekere, Omer C. Onar, Jason L. Pries

October 2020

The INL is a U.S. Department of Energy National Laboratory
operated by Battelle Energy Alliance

INL/CON-19-56932-Revision-1

Electromagnetic Shielding Design for 200 kW Stationary Wireless Charging of Light-Duty EV

Bo Zhang, Richard Barney Carlson, Veda P. Galigekere, Omer C. Onar, Jason L. Pries

October 2020

Idaho National Laboratory
Idaho Falls, Idaho 83415

http://www.inl.gov

Prepared for the
U.S. Department of Energy
Office of Energy Efficiency and Renewable Energy
Under DOE Idaho Operations Office
Contract DE-AC07-05ID14517

Electromagnetic Shielding Design for 200 kW Stationary Wireless Charging of Light-Duty EV

Bo Zhang
Department of Energy Storage and Advanced Transportation
Idaho National Laboratory
Idaho Falls, ID USA
bo.zhang@inl.gov

Richard B. Carlson
Department of Energy Storage and Advanced Transportation
Idaho National Laboratory
Idaho Falls, ID USA
richard.carlson@inl.gov

Veda P. Galigekere
National Transportation Research Center
Oak Ridge National Laboratory
Knoxville, TN USA
galigekerevn@ornl.gov

Omer C. Onar
National Transportation Research Center
Oak Ridge National Laboratory
Knoxville, TN USA
onaroc@ornl.gov

Jason L. Pries
National Transportation Research Center
Oak Ridge National Laboratory
Knoxville, TN USA
priesjl@ornl.gov

***Abstract*—Wireless power transfer (WPT) is a developing technology with the advantage of convenience and flexible charging. SAE recommended practice J2954 defines typical size and geometry with aluminum or ferrite plate shielding to limit leakage electromagnetic (EM) fields for WPT with power levels lower than 22 kVA from the input side. However, as the WPT power goes up to 100- or 200-kW level, EM safety surrounding the WPT becomes a critical concern. To address this oncoming safety challenge, a novel ferrite shielding design is proposed in this paper. Different misalignment scenarios in accordance with definitions in SAE J2954 are also taken into consideration to ensure EM safety under various operation scenarios. Simulation results, which are preliminarily verified by magnetic field measurements at 1.1 m from the center of the vehicle side coil under 100 kW operation, indicate that the magnetic field leakage can be maintained below the limits defined in SAE J2954 for 200 kW operation. A 3.3 kW scale-down test was also carried out and compared to parallel scale-down simulations. 26.8% field emission reduction is observed from the scale-down test, which supports the effectiveness of the proposed shielding design.**

Keywords—wireless power transfer, inductive power transfer, electric vehicle, electromagnetic field, ferrite shielding

I. Introduction

Wireless Power Transfer (WPT) or inductive power transfer (IPT) promises convenient, autonomous, and highly efficient charging of electric vehicles (EVs) [1]-[4]. SAE recommended practice J2954 [5] defines typical size and geometry with aluminum or ferrite plate shielding to limit leakage electromagnetic fields, which works well for WPT with power levels up to 22 kVA from the input side. However, as the WPT power increases to 100 or 200 kW level [6]-[8], electromagnetic (EM) safety in regard to human health surrounding the WPT becomes a critical concern [9], [10].

Numerous existing investigations of WPT coil pad designs and optimizations have mainly focused on improving power transfer efficiency and tolerance of misalignment [11]-[14]. In terms of suppressing leakage magnetic field, a bipolar pad with appropriate energization was used to control field emission under misalignment condition in [15]. Several shapes of ferrites together with auxiliary cancellation winding designs were proposed to actively mitigate leakage flux [16]. A hybrid shield consisting of a thin aluminum plate and a copper shield-ring was presented to improve shielding effectiveness [17]. Magnetic field patterns with different coil pad structures were compared in [18]. These methodologies are effective solutions to mitigate field emissions of WPT systems with operational power less than 22 kVA. But, aiming at 200 kW WPT integrated into a light-duty EV (LDEV), advanced shielding solutions are required to ensure electromagnetic safety.

This paper presents a novel shield design for a 200 kW WPT system which is going to be integrated into an LDEV. EM safety standards and challenges, shielding considerations, design details, and simulations are presented in the following sections. Laboratory scale-down tests are also carried out with a 3.3 kW WPT system, which preliminarily validate the shielding effectiveness. Given the different technical features, this paper focuses on a high-power WPT for LDEVs; and the discussion of HDVs (e.g., trains, buses) [19]-[21] is beyond the scope of this paper.

II. Magnetic Field Safety Challenge for High Power Wireless Power Transfer

A. Standards and Criteria Definitions

SAE recommended practice J2954 entitled "Wireless Power Transfer for Light-Duty Plug-In/Electric Vehicles and Alignment Methodology" [5] defines the electromagnetic field (EM) emission regions for LDEV, as shown in Fig. 1. According to [5], magnetic and electric fields on boundaries between region 1 and 2, as shown in Fig. 1 (a), should comply with International Commission on Non-Ionizing Radiation Protection Guidelines 2010 (ICNIRP 2010) [22]. For LDEV, the distance from boundaries to the coupler center is defined as 0.8 m, which is derived from the width of a 1.6-m wide compact LDEV [5]. The direction for these criteria are along the *y*-direction, as shown in Fig. 1 (b) based on [5] in accordance with ISO 4130 [23]. In this paper, all magnetic field simulation curves versus distance to the center of coils are along *y*-direction. Also, only stationary WPT is investigated in this paper. Dynamic WPT for in-motion charging is not discussed here since the current EM safety criteria from SAE J2954 are for stationary charging only, and the criteria for in-motion charging is still under discussion [24].

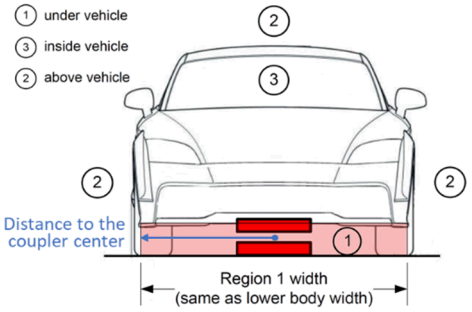

(a)

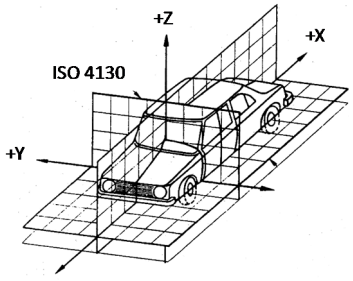

(b)

Fig. 1. Definition of magnetic field emission limitations for LDEV in SAE J2954. (a) regions and limits (b) directions [5].

ICNIRP 2010 defines the permitted exposure for both electric and magnetic fields. For WPT in the frequency range between 3 kHz and 100 kHz, allowed exposure level is 27 μT for magnetic field and 83 V/m for electric field. According to a recent published test and evaluation from 25 kW WPT, electric field generated by WPT is typically less than 10% of the required limit 83 V/m [25]. Therefore, the magnetic field constraint is the main consideration. This study specifically focuses on magnetic field, while electric field is beyond the scope of this paper and will be investigated in the future work for the 200 kW power transfer condition.

B. Challenges

As the WPT power goes up, electromagnetic safety surrounding the WPT becomes a critical concern for both human health and environment protection. SAE J2954 [5] also defines the recommended shielding design by utilizing aluminum plate with a dimension of 800 × 800 × 0.7 mm or larger for WPT up to 11.1 kVA. For WPT around 20 kW, ferrite backing plate shielding is the main solution [26]. However, for power level higher than 100 kW, or even up to 200 kW, ensuring electromagnetic safety with the constraints of LDEV space limitation is an emerging challenge. Table I summaries typical shielding designs with different power levels [10]. WPT1 to WPT4 based on the input power from the grid in kVA units as well as relevant typical shielding solutions mentioned in Table I are in accordance with definitions in recommended practice SAE J2954.

TABLE I [5], [10]
TYPICAL PASSIVE SHIELDING SOLUTIONS FOR WPT WITH DIFFERENT POWERS

Power	Shielding material	Impact on efficiency	Weight/ size
3.7 kVA (WPT1)	aluminum plate	low	low
7.7 kVA (WPT2)	aluminum plate	low	low
11.1 kVA (WPT3)	aluminum plate	low	low
22 kVA (WPT4)	ferrite plate	very low (<1% reduction)	medium
22-120 kVA	ferrite plate	very low (<1% reduction)	medium

As a typical example of high power WPT, an 100 kW WPT system, with parameters referring to [6], [8] as shown in Table II, is adopted here to present the magnetic field increases along with the increasing power levels. A three-dimensional (3D) finite-element model developed in COMSOL is utilized for this simulation. Note that the "DD" type coil mentioned in Table II is also consistent with definition in SAE J2954 and references [6], [8].

TABLE II
100 KW WPT COIL PARAMETERS

Quantity	Value [unit]
Resonant frequency	22 [kHz]
output power	100 [kW]
ground-side current	177 [A]
vehicle-side current	171 [A]
turns of ground or vehicle-side coil	8
air-gap	125 [mm]
external dimension	825×609×33mm
coil type	DD
shielding design	backing ferrite

Fig. 2 [10] presents the simulated magnetic field results versus distances to the center of coils along *y*-direction mentioned in Fig. 1(b) with a transferred power from 100 kW to 350 kW. A measured magnetic field result of 21.64 μT at 1.1 m is also presented as a preliminary verification of

simulation models. In Fig. 2, with an increase of power from 100 to 350 kW, the magnetic field increases significantly. Taking the distance of 0.8 m as the criteria that was discussed previously in subsection II. A, the magnetic field emission with 100 kW or higher power already exceeds the magnetic field limitation of 27 μT according to ICNIRP 2010 [22] if no further field shielding method is utilized.

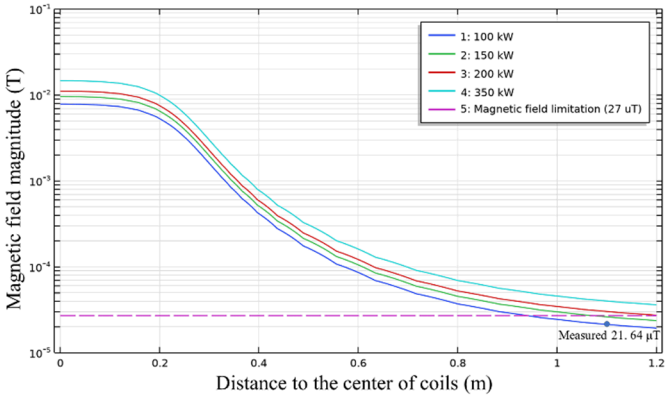

Fig. 2. Magnetic field magnitude versus the distance to the center of coils with operated powers from 100 to 350 kW [10].

III. WPT Features, Equations and EM Safety Considerations

A. WPT Circuit and Equations

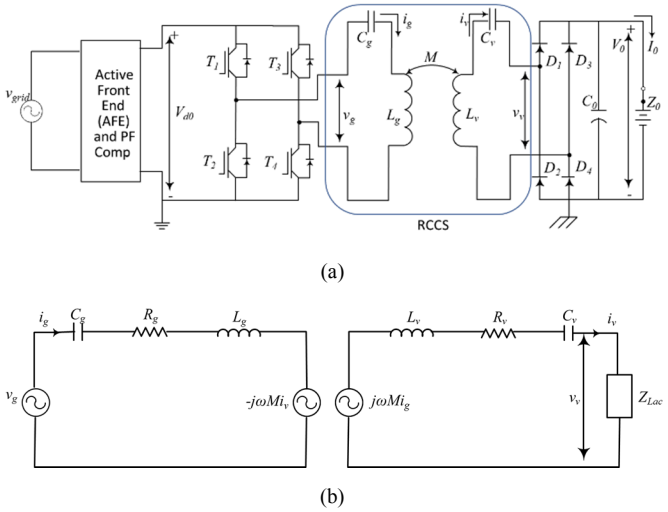

Fig. 3. (a) The example 100 kW wireless power transfer circuit schematic, and (b) resonance circuit and coil system (RCCS) equivalent circuit.

Fig. 3(a) shows the example 100 kW WPT circuit with parameters referring to [6], [8]. It consists of grid voltage input, active front-end rectifier with power factor correction, ground side high-frequency inverters, resonance circuit and coil system (RCCS), vehicle side rectifier, and battery load. For RCCS, the equivalent circuit is shown in Fig. 3(b), where v_g, i_g, C_g, R_g, and L_p present the ground side voltage, current, compensation capacitor, coil resistance, and coil self-inductance; v_v, i_v, C_v, R_v, and L_v present the vehicle side voltage, current, compensation capacitor, coil resistance, and coil self-inductance. In Fig. 3(a), V_0 is the vehicle-side DC output voltage and M the mutual inductance between ground- and vehicle-side coils. The DC load Z_0 in Fig. 3(a) can be transferred to AC side equivalent resistor Z_{Lac} in Fig. 3(b) as below [27], [28],

$$Z_{\mathrm{Lac}} = \frac{8}{\pi^2} Z_0 \tag{1}$$

Similarly, v_v can also be given as:

$$\mathrm{v}_v = \frac{2\sqrt{2}}{\pi} V_0 \tag{2}$$

Circuit equations based on RCCS equivalent circuit shown in Fig. 3(b) can be given by:

$$\mathrm{v}_g = \left(j\omega L_g + \frac{1}{j\omega C_g} + R_g\right) i_g - j\omega M i_v \tag{3}$$

$$j\omega M i_g = \left(j\omega L_v + \frac{1}{j\omega C_v} + R_v + Z_{Lac}\right) i_v \tag{4}$$

where the mutual inductance M is given by:

$$M = k\sqrt{L_g L_v} \tag{5}$$

where k is coupling coefficient typically between 0.1 to 0.5 owing to the loosely coupling [29].

Considering the resonant circuit, L_g, L_v, C_g, and $\mathrm{C_v}$ are in resonance at the angular frequency ω_0, which meets the following equations:

$$j\omega_0 L_g + \frac{1}{j\omega_0 C_g} = j\omega_0 L_v + \frac{1}{j\omega_0 C_v} = 0 \tag{6}$$

Assuming that R_v is negligible compared to Z_{Lac}, the output power on the vehicle side can be written as:

$$P_0 = v_v i_v = \omega M I_g I_v sin\varphi_{gv} \tag{7}$$

where I_g, I_v are the RMS values of the ground- and vehicle-side currents, respectively; and $sin\varphi_{gv}$ is the power factor on the vehicle side. Noting that there are also many other advanced compensation power electronics topologies different from Fig. 3(a) (e.g., LCC-LCC circuit), but Eq. (7) is still applicable as a general equation considering the electromagnetic to electric energy conversion regardless of specific circuit topologies. Ideally, when the vehicle side resonant circuit is fully compensated, as shown in Eq. (6), the power factor in Eq. (7) equates to 1.

B. EM Safety Considerations

To ensure EM safety, magnetic field emission must be considered, which comply with recommended practice SAE J2954 [5] (0.8 m distance criteria) and ICNIRP 2010 [30] (27 μT magnetic field criteria), respectively, as mentioned in previous subsection II. A.

Misalignment is another critical concern which makes EM safety issues even more challenging, as discussed in [10]. SAE J2954 also defines the allowed maximum misalignments

between ground- and vehicle-side coils, which should be no more than 75 mm in *x*-direction and no more than 100 mm in *y*-direction (*x* and *y*-directions defined in Fig. 1(b)), with length of coils (if applicable) specified along the travel direction [5]. To ensure EM safety, the worst case of maximum misalignment is taken into account in this paper.

This study focuses on ferrite plate shielding, which leads to losses. However, due to the high ferrite resistance, eddy current losses within ferrite materials are typically quite low at operating frequencies of 10 kHz to 100 kHz [31], [32]. Therefore, no specific ferrite shape design is discussed here for the purpose of mitigating eddy current, and the ferrite loss is mainly determined by ferrite's own characteristics as well as the operating power.

Integrating shielding into the WPT system leads to changes in the self-inductances and the mutual inductance. To ensure maximum power factor according to Eqs. (6) and (7), compensation capacitors on both ground and vehicle sides need to be re-tuned after shielding is integrated. For light-duty EV application, weight and size should also be minimized for a compact coil design.

IV. "WING" TYPE SHIELD DESIGN

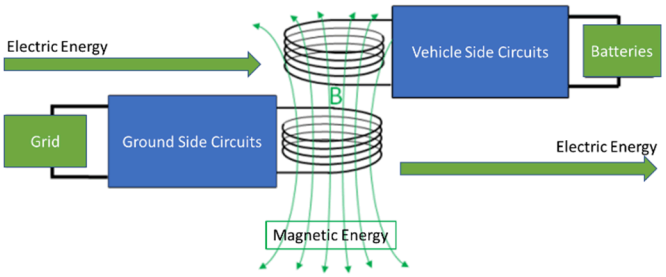

Fig. 4. Energy conversion process of WPT.

Based on the energy conversion mechanism of WPT, the grid side electric energy is converted to electromagnetic energy first, and then converted back to electric energy on the vehicle side to charge the batteries, as shown in Fig. 4. The electromagnetic energy exists in the form of 3D magnetic fields generated by ground- and vehicle-side coils. Assuming the coupler losses, which consist of copper and ferrite losses in both ground side and vehicle side, are identical on the ground and vehicle sides, the energy conversion process can be written as,

$$E_{grid} = E_g + 0.5E_{coup} + E_{mag} \tag{8}$$

$$E_{mag} = E_v + 0.5E_{coup} + E_{bat} \tag{9}$$

where E_{grid}, E_{mag}, and E_{bat} present the energy from grids, the one stored in magnetic field, and the one goes to battery; E_g, E_v, and E_{coup} are ground side circuit, vehicle side circuit and coupler energy losses, respectively.

Magnetic energy distributed in a 3D space can be calculated as:

$$E_{mag} = \frac{1}{2}\iiint_{global}\frac{B^2}{\mu}dV \tag{10}$$

where *global* means that the integration must be implemented in the whole space where magnetic flux exists; μ is the permeability of different materials in the proposed integration elements; and B is the relevant magnetic flux density magnitude in the same integration elements as μ.

Theoretically, for a given WPT system with a certain output power requirement and a certain loss percentage of the total energy, E_{mag} is also a fixed value as described in Eqs. (8) and (9); regardless of coils or ferrites shape. Hence, the strategy of shielding design in this paper is to shape the field and centralize field distributions as much as possible, so that the field density increases in the center and its leakage at 0.8 m decreases given a fixed total amount of electromagnetic energy, as shown in Fig. 5.

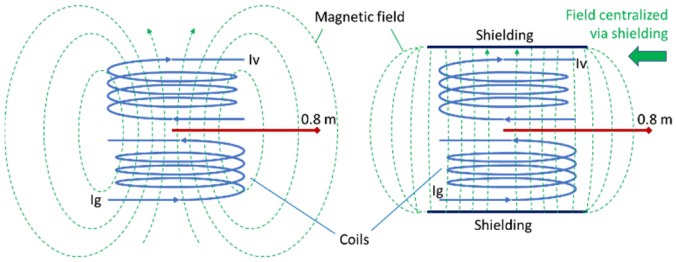

Fig. 5. (a) Magnetic field distribution without shielding and (b) field centralized after shield applied.

Fig. 6 presents the proposed shielding design process for a high power (100-200 kW level) WPT application, including the proposed design (Fig. 6(e)). Fig. 6(a) presents the example 120 kW WPT coils and shielding design with geometry parameters referring to [6], [8]. To centralize fields and reduce emission, ferrite teeth are added on the edges of both ground and vehicle side backing ferrites, as shown in Fig. 6(b) and (c). To ensure EM safety in the case of misalignment, as defined by SAE J2954 [5] and discussed in Subsection III. B, back ferrites are extended as shown in Fig. 6(d). Due to the anisotropy field distribution created by DD coils, back ferrites are further designed with extension only in *y*-direction for size and weight consideration, shown in Fig. 6(e) as the proposed shielding design. Since the shielding appears as a "wing" in shape, it is called "wing" type shielding design in this paper. Relevant effectiveness, impact, and sensitive analysis are discussed in the following sections.

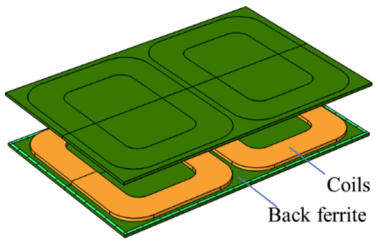

(a)

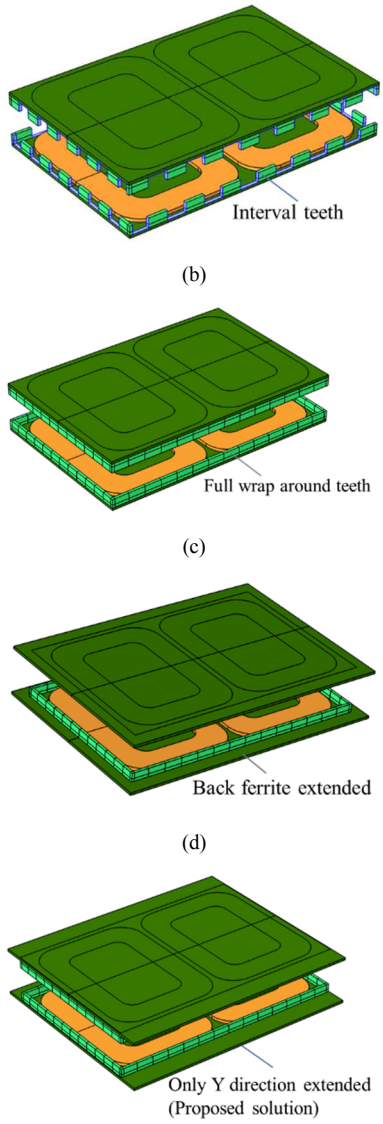

Fig. 6. Proposed shielding design for high power WPT applications. (a) Original back ferrite shielding, (b) interval teeth added, (c) full wrap around teeth added, (d) back ferrite extended for misalignment tolerance, and (e) proposed design for stationary high power WPT.

V. Effectiveness, Impact and Sensitive Analysis

A. *Shielding Effectiveness without Considering Misalignments*

To reduce magnetic field emission, a novel "teeth" design, as shown in Fig. 3(b), centralizes the field and suppresses emissions. 3C95 Ferrite from Ferroxcube is the preferred ferrite shielding material in this study due to its high resistance (5 Ω·m) in mitigating eddy current losses and high relevant permeability (3000 at 25□) in conducting magnetic field.

There might be an obvious concern with this "teeth" type shielding design that the "teeth" actually reduces the magnetic distance [5] between ground and vehicle-side coils. Therefore, to minimize the impact on reducing magnetic distance, the *z*-direction height of teeth is carefully selected. Referring to [6], [8], 2AWG Litz wires are utilized to wire the single layer DD coil with a wire diameter of 11.2 mm. Considering the amount and dimension availability of ferrite plate, 38×25×3.8 mm ferrite plates are selected to fabricate the "teeth" with 25 mm in z-direction. Assuming the original air gap as shown in Fig. 6(a) is 125 mm, referring to [6], the magnetic distance is reduced from 125 mm to 97.4 mm after "teeth" added, which is still acceptable for prototype level development.

Fig. 7 presents the simulated magnetic field suppression comparison between back shielding and teeth shielding. The blue line in Fig. 7 is a baseline with 100 kW operation power, which is preliminarily verified by one-point magnetic field measurement at 1.1 m. From 100 kW to 200 kW, magnetic field at 0.8 m increases from 37.2 μT to 52.6 μT, which are both above the 27 limitation of the ICNIRP guideline. After interval or full wrap around teeth are added, magnetic field emission reduces significantly to 24.3 uT and 16.3 uT, which are below the ICNIRP 2010 exposure limit.

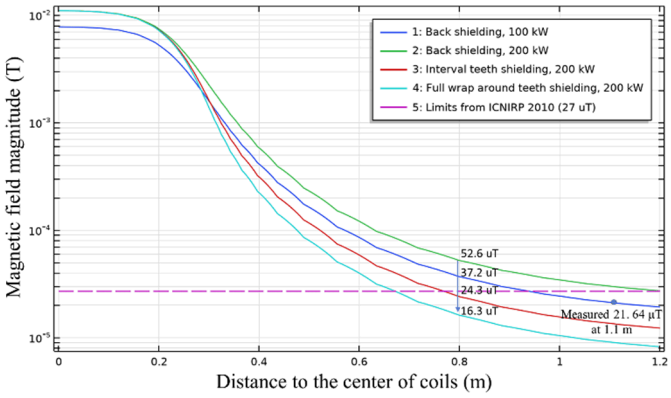

Fig. 7. Magnetic field suppressing effectiveness with teeth shielding.

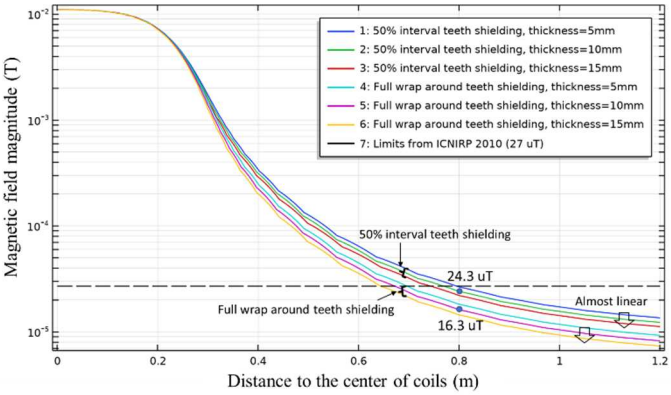

Fig. 8. Sensitive analysis with different teeth dimensions.

To understand teeth dimensional impacts on shielding effectiveness, sensitivity analysis simulations are conducted with different teeth thicknesses in full wrap around or a 50% interval partition teeth shielding, as shown in Fig. 8. The line No. 2 and No. 5 in Fig. 8 are two baselines with 10 mm thickness teeth shielding, which are aligned with the red and light blue results shown in Fig. 7. It is observed that the effectiveness of suppressing stray magnetic field is almost a linear reduction from 50% interval teeth shielding to full teeth

shielding, along with similar linear reduction trend in terms of different teeth thicknesses. In terms of weight/size consideration aspect, adding 10 mm teeth only increases the weight by 4.2% - 8.4% compared to typical back shielding, which also makes it beneficial for practical applications despite of an acceptable reduction in magnetic distance between coils.

B. Shielding Considering Misalignments

SAE J2954 defines the allowed maximum misalignments between ground and vehicle coils, as mentioned in Subsection III. B [5]. In case of maximum misalignments, magnetic field emissions drastically increase.

3-D electromagnetic simulation has been carried out to analyze the magnetic field distribution with and without misalignments, as shown in Fig. 9, with parameters still referring to Table II. The rainbow color slice presents magnetic field distribution in the middle *x*-*y* plane, and the 3-D flying red arrows represent the direction and magnitude of magnetic fields in a nearby 3-D volume. Comparing Fig. 9(b) to (a), it is obvious that misalignment does lead to an obvious field distortion. The original magnetic field distribution without misalignment shown in Fig. 9(a) is fully symmetric in *x*-*y* plane, but it tends to distort in an "L" shape towards the misalignment direction shown in Fig. 9(b), which significantly changes the field shape, stray field, and the maximum field magnitudes.

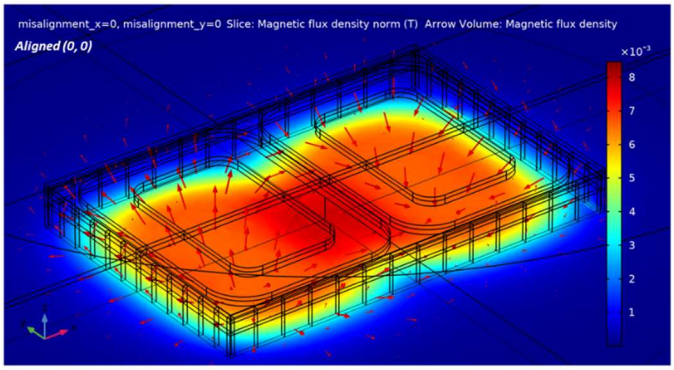

(a)

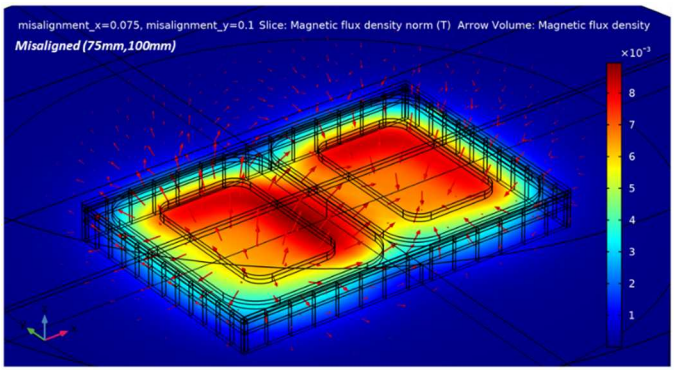

(b)

Fig. 9. 3-D magnetic field distribution (a) without misalignment and (b) with maximum misalignment.

Assuming that the coupling factor's reduction due to misalignment is negligible which is the ideal case for power transfer but the worst case for EM safety theoretically (EM safety won't be a concern if the coupling factor reduces to 0), Fig. 10 presents the magnetic field along *y*-direction with different misalignments. Noting that 0 distance center in Fig. 10 is always aligned with vehicle-side coil center according to the definition in SAE J2954 [5]; this misalignment leads to dissymmetric field distributions along *y*-direction. The light blue line No. 4 in Fig. 10 is a baseline which is aligned with the blue result shown in Fig. 7. Considering the theoretically worst case for EM safety design where the coupling factor won't reduce with misalignments, misalignment increases magnetic field significantly from 37.2 μT to 70.2 μT at 0.8 m when operated at 100 kW.

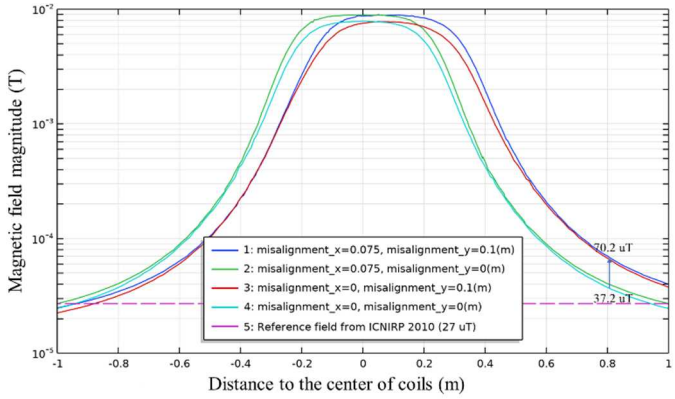

Fig. 10. Magnetic field along y-direction with different misalignments.

Fig. 10 also indicates that stray magnetic field along *y*-direction is more sensitive to y-direction misalignment instead of *x*-direction misalignment, especially with DD coils which creates an anisotropic field distribution. Hence, to suppress misalignment's impacts, additional *y*-direction extend in back ferrite is adopted, as shown in Fig. 6(e). Fig. 11 presents the shielding effectiveness comparison with and without *y*-direction back ferrite extension, where the blue is a baseline that is consistent with the light blue result in Fig. 7. Comparing the green line and red line in Fig. 11, *y*-extension significantly reduces the field emission from 41.0 μT to 23.8 μT at 0.8 m, which is now under the limits based on ICNIRP 2010. The *y*-extension utilized here is 150 mm compared to 609 mm original width of back ferrite. The total weight increasement including teeth and back ferrite extension is 28.9% compared to original 825×609×20 mm ferrite [6], which is still acceptable.

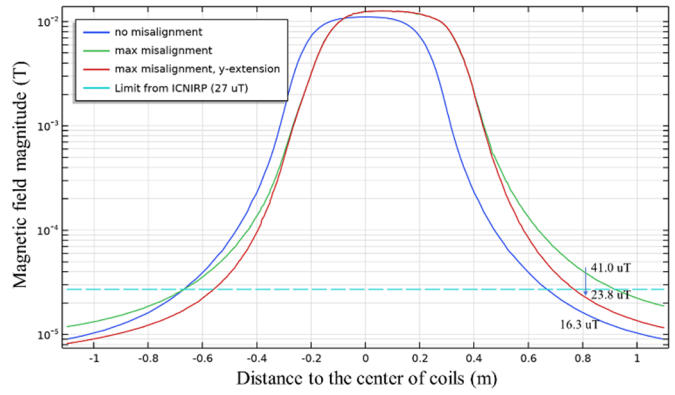

Fig. 11. Magnetic field suppress effectiveness along y-direction with maximum misalignments and 200 kW operation.

VI. Scale-down Tests

Scale-down experiments with the available 3.3 kW WPT in the lab are carried out to test the shielding effectiveness with 50% interval teeth. A series of magnetic field points from 400 mm to 1 m away from the coils' center are measured with the proposed interval teeth shielding and baseline back ferrite shielding. A precise magnetic field measurement platform consists of servo-motors, a non-metallic platform, positioning system, Hioki magnetic field probe, and Labview data acquisition system is utilized to measure the field distributions and test the effectiveness of the shielding, as shown in Fig. 12.

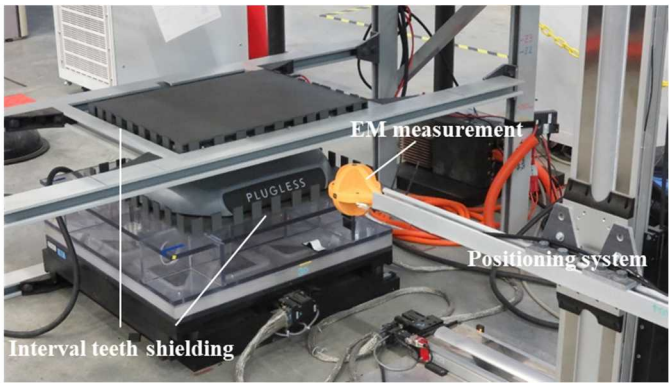

Fig. 12. EM testing plarfom set up.

Fig. 13 presents the measured and simulated magnetic field reduction with and without the proposed interval teeth shielding. The 3.3 kW system utilizes smaller circular coils that are different from the full-size DD ones mentioned in previous analyses; therefore, the simulation model is also concurrently adjusted to the size of the smaller tested coils as well as power level. The adjusted scale-down simulation results shown with red and orange lines in Fig. 13 match well with the measured results despite some minor errors at 1 m due to 3-D mesh quality reduction in far-field finite-element simulations. Based on the test, magnetic field emission at 0.8 m reduces from 6.6 to 4.8 μT (26.9% reduction), which partially supports the effectiveness of teeth shielding.

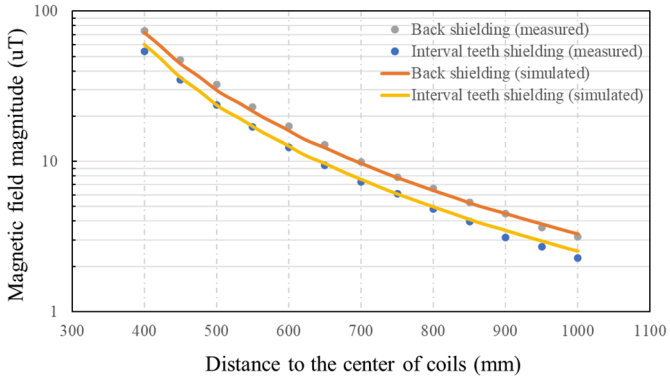

Fig. 13. Measured and simulated results with and without proposed teeth shielding.

VII. Conclusion and Discussion

A "wing" shape passive ferrite shielding for stationary high power WPT is presented in this paper, which is designed to ensure EM safety in case of maximum misalignments for 200 kW WPT operation. Simulation results indicate the shielding effectiveness, which can maintain field emission under limitations in accordance with SAE J2954. Scaled down in-lab test is also carried out with a 3.3 kW WPT system. 26.9% field emission reduction is observed with interval teeth shield added based on test results, which also supports the effectiveness of the proposed design.

Currently, the in-lab EM scan testing platform is under improvement at Idaho National Laboratory to perform EM safety evaluations in misalignments scenarios, larger coupler sizes as well as higher operation powers. A 200 kW dynamic WPT hardware device integrated with LDEV is also under development, which is led by Oak Ridge National Laboratory, in partnership with Idaho National Laboratory. The goal is to achieve real in-motion/ stationary 200 kW WPT for LDEV while ensuring EM safety during charging. Future work will include DD coil EM testing, power electronics circuit design, and overall WPT system operation.

Acknowledgment

This work was supported by the U.S. Department of Energy (DOE), Vehicle Technologies Office, under the project FY2019 VTO AOI 3B: "High Power and Dynamic Wireless Charging for Electric Vehicles," with collaborative partnership between Oak Ridge National Laboratory and Idaho National Laboratory. Authors thank Lee Slezak from U.S. DOE for project oversight and technical leadership.

References

[1] C. T. Rim and C. Mi, Wireless power transfer for electric vehicles and mobile devices. John Wiley & Sons, 2017.

[2] D. Patil, M. Mcdonough, J. Miller, B. Fahimi, and P. Balsara, "Wireless Power Transfer for Vehicular Applications: Overview and Challenges,", IEEE Transactions on Transportation Electrification, Article vol. 4, no. 1, pp. 3-37, MAR 2018.

[3] Z. Zhang, H. Pang, A. Georgiadis, and C. Cecati, "Wireless Power Transfer-An Overview,", IEEE Transactions on Industrial Electronics, Article vol. 66, no. 2, pp. 1044-1058, FEB 2019.

[4] G. Covic and J. Boys, "Inductive Power Transfer,", Proceedings of the IEEE, Article vol. 101, no. 6, pp. 1276-1289, JUN 2013.

[5] SAEJ2954. "Wireless Power Transfer for Light-Duty Plug-in/Electric Vehicles and Alignment Methodology." [online] available: https://www.sae.org/standards/content/j2954_201904/. (accessed June 1, 2020).

[6] V. P. Galigekere et al., "Design and Implementation of an Optimized 100 kW Stationary Wireless Charging System for EV Battery Recharging," in 2018 IEEE Energy Conversion Congress and Exposition (ECCE), 23-27 Sept. 2018, pp. 3587-3592.

[7] C. Zhang, S. Srdic, S. Lukic, Y. Kang, E. Choi, and E. Tafti, "A SiC-Based 100 kW High-Power-Density (34 kW/L) Electric Vehicle Traction Inverter," in 2018 IEEE Energy Conversion Congress and Exposition (ECCE), 23-27 Sept. 2018, pp. 3880-3885.

[8] J. Pries et al., "Coil Power Density Optimization and Trade-off Study for a 100kW Electric Vehicle IPT Wireless Charging System," in 2018 IEEE Energy Conversion Congress and Exposition (ECCE), 23-27 Sept. 2018, pp. 1196-1201.

[9] S. Park, "Evaluation of Electromagnetic Exposure During 85 kHz Wireless Power Transfer for Electric Vehicles,", IEEE Transactions on Magnetics, Article vol. 54, no. 1, JAN 2018, Art no. ARTN 5100208.

[10] B. Zhang, R. B. Carlson, J. G. Smart, E. J. Dufek, and B. Liaw, "Challenges of Future High Power Wireless Power Transfer for Light-duty Electric Vehicles----Technology and Risk Management," eTransportation, vol. 2, p. 100012, 2019.

[11] A. Azad, A. Echols, V. Kulyukin, R. Zane, and Z. Pantic, "Analysis, Optimization, and Demonstration of a Vehicular Detection System Intended for Dynamic Wireless Charging Applications,", IEEE Transactions on Transportation Electrification, Article vol. 5, no. 1, pp. 147-161, MAR 2019.

[12] L. Zhao, D. Thrimawithana, U. Madawala, A. Hu, and C. Mi, "A Misalignment-Tolerant Series-Hybrid Wireless EV Charging System With Integrated Magnetics,", IEEE Transactions on Power Electronics, Article vol. 34, no. 2, pp. 1276-1285, FEB 2019.

[13] A. Mohamed, S. An, and O. Mohammed, "Coil Design Optimization of Power Pad in IPT System for Electric Vehicle Applications,", IEEE Transactions on Magnetics, Article vol. 54, no. 4, APR 2018, Art no. ARTN 9300405.

[14] Y. Li et al., "A New Coil Structure and Its Optimization Design With Constant Output Voltage and Constant Output Current for Electric Vehicle Dynamic Wireless Charging," IEEE Transactions on Industrial Informatics, vol. 15, no. 9, pp. 5244-5256, 2019.

[15] F. Lin, G. Covic, and J. Boys, "Leakage Flux Control of Mismatched IPT Systems,", IEEE Transactions on Transportation Electrification, Article vol. 3, no. 2, pp. 474-487, JUN 2017.

[16] S. Choi, B. Gu, S. Lee, W. Lee, J. Huh, and C. Rim, "Generalized Active EMF Cancel Methods for Wireless Electric Vehicles,", IEEE Transactions on Power Electronics, Article vol. 29, no. 11, pp. 5770-5783, NOV 2014.

[17] M. Mohammad, E. Wodajo, S. Choi, and M. Elbuluk, "Modeling and Design of Passive Shield to Limit EMF Emission and to Minimize Shield Loss in Unipolar Wireless Charging System for EV,", IEEE Transactions on Power Electronics, Article vol. 34, no. 12, pp. 12235-12245, DEC 2019.

[18] A. Ahmad, M. S. Alam, and A. A. S. Mohamed, "Design and Interoperability Analysis of Quadruple Pad Structure for Electric Vehicle Wireless Charging Application," IEEE Transactions on Transportation Electrification, pp. 1-1, 2019.

[19] J. Shin et al., "Design and Implementation of Shaped Magnetic-Resonance-Based Wireless Power Transfer System for Roadway-Powered Moving Electric Vehicles,", IEEE Transactions on Industrial Electronics, Article vol. 61, no. 3, pp. 1179-1192, MAR 2014.

[20] R. Bosshard and J. Kolar, "Multi-Objective Optimization of 50 kW/85 kHz IPT System for Public Transport,", IEEE Journal of Emerging and Selected Topics in Power Electronics, Article vol. 4, no. 4, pp. 1370-1382, DEC 2016.

[21] K. Hwang, J. Cho, J. Park, D. Har, and S. Ahn, "Ferrite Position Identification System Operating With Wireless Power Transfer for Intelligent Train Position Detection,", IEEE Transactions on Intelligent Transportation Systems, Article vol. 20, no. 1, pp. 374-382, JAN 2019.

[22] I. C. Non-Ionizing and I. C. Non-Ionizing, "ICNIRP Statement-Guidelines for limiting exposure to time-varying electric and magnetic fields (1 Hz to 100 kHz),", Health Physics, Article vol. 99, no. 6, pp. 818-836, DEC 2010.

[23] ISO4130. "Road Vehicles - Three-Dimensional Reference System and Fiducial Marks - Definitions." [online] available: https://www.iso.org/standard/9886.html. (accessed June 1, 2020).

[24] B. Zhang et al., "Concept Design of Active Shielding for Dynamic Wireless Charging of Light-duty EV," in 2020 IEEE Transportation Electrification Conference and Exposition (ITEC), 22-26 June 2020, pp.1-7.

[25] A. Mohamed, A. Meintz, P. Schrafel, and A. Calabro, "Testing and Assessment of EMFs and Touch Currents From 25-kW IPT System for Medium-Duty EVs,", IEEE Transactions on Vehicular Technology, Article vol. 68, no. 8, pp. 7477-7487, AUG 2019.

[26] O. C. Onar, M. Chinthavali, S. L. Campbell, L. E. Seiber, C. P. White, and V. P. Galigekere, "Modeling, Simulation, and Experimental Verification of a 20-kW Series-Series Wireless Power Transfer System for a Toyota RAV4 Electric Vehicle," in 2018 IEEE Transportation Electrification Conference and Expo (ITEC), 13-15 June 2018, pp. 874-880.

[27] V. Vorperian, "Simplified analysis of PWM converters using model of PWM switch. Continuous conduction mode,", IEEE Transactions on Aerospace and Electronic Systems, Article vol. 26, no. 3, pp. 490-496, MAY 1990.

[28] H. Wu, A. Gilchrist, K. Sealy, and D. Bronson, "A High Efficiency 5 kW Inductive Charger for EVs Using Dual Side Control,", IEEE Transactions on Industrial Informatics, Article vol. 8, no. 3, pp. 585-595, AUG 2012.

[29] V. Jiwariyavej, T. Imura, and Y. Hori, "Coupling Coefficients Estimation of Wireless Power Transfer System via Magnetic Resonance Coupling Using Information From Either Side of the System,", IEEE Journal of Emerging and Selected Topics in Power Electronics, Article vol. 3, no. 1, pp. 191-200, MAR 2015.

[30] I. C. Non-Ionizing, "ICNIRP Statement-Guidelines for limiting exposure to time-varying electric and magnetic fields (1 Hz to 100 kHz),", Health Physics, Article vol. 99, no. 6, pp. 818-836, DEC 2010.

[31] KEMET. [online available]: https://www.kemet.com/en/us/emc/ferrite-materials.html. (accessed June 1, 2020).

[32] Ferroxcube. [online] available: https://www.ferroxcube.com/en-global/ak_material/index/power_conversion#5. (accessed June 1, 2020).